Identifying Substrate-Dependent Chemical Bonding Nature at Molecule/Metal Interfaces Using Vibrational Sum Frequency Generation Spectroscopy and Theoretical Calculations

Ben Wang,[†] Mikio Ito,[#] Min Gao,[§] Hidenori Noguchi,[$]

Kohei Uosaki,[$,*] and Tetsuya Taketsugu[†,‖,*]

[†]*Department of Chemistry, Faculty of Science, Hokkaido University, Sapporo 060-0810, Japan*

[#]*Department of Chemical Science and Engineering, National Institute of Technology, Tokyo College, 1220-2 Kunugida-machi, Hachioji, Tokyo 193-0997, Japan*

[§]*Institute for Catalysis, Hokkaido University, Sapporo 001-0021, Japan*

[$]*Center for Global Research on Energy and Environmental Materials (GREEN), National Institute for Materials Science (NIMS), Tsukuba 305-0044, Japan*

[‖]*Institute for Chemical Reaction Design and Discovery (WPI-ICReDD), Hokkaido University, Sapporo 001-0021, Japan*

Abstract

The effect of the metal substrate on the chemical bonding nature at the molecule-metal interface was investigated for aryl isocyanide molecules with different para-substituents X−C_6H_4−NC (X = H; NO_2 (electron-donating group); OCH_3 (electron-withdrawing group)) adsorbed on Au(111) and Ag(111) surfaces by surface-specific vibrational sum frequency generation (VSFG) spectroscopy and periodic density functional theory calculations. Both the experimental VSFG spectra and the anharmonic vibrational spectra from theoretical calculations confirm that the substrate effect acts to increase the NC stretching frequency (blue shift) and that the Au(111) surface shows a larger blue shift than the Ag(111) surface. To analyze the mechanism of this substrate dependence, we performed a natural bond orbital (NBO) analysis extended to periodic systems, and found that at the molecule-metal interface, the σ donation from molecule to substrate (strengthening NC bond) is more pronounced than the π back-donation (weakening NC bond), and that the effect of σ donation is stronger for the Au substrate than for the Ag substrate.

1. Introduction

Chemical bonding interactions between organic molecules and metal surfaces determine many interfacial phenomena, such as charge transport,[1−4] dynamics of electronic and vibrational excitations,[5,6] chemical reactivity[7,8] in the interfacial region between metal electrodes. Characterization of these interfacial bonds plays an important role in surface modification and functionalization. However, it is challenging to characterize the adsorption structure of molecules on the surface because of its complexity including the adsorption sites and the problems of surface coverage and orientation. Well-ordered self-assembled monolayer (SAM) on metal electrode, an essential component of molecular electronic devices, is a typical model for studying adsorbent−substrate interactions.[9,10] Charge transfer between the SAM and the metal electrode strongly depends on the surface topography of the metal electrode. Therefore, it is necessary to understand how the intrinsic properties of the metal surface affect the interface structure before implementing the SAM for a particular application. Because of the strong chemical bonding between the −S group and the atoms on the gold surface, thiol compounds on gold surfaces are one of the most investigated systems.[11−19] Aryl isocyanide molecules are also important candidates because of the effective network of delocalized electrons between the π-orbitals of the benzene ring and the d-band of the metal surface, linked by triple bonds of NC groups, and therefore have been studied extensively.[20−30] The interaction of aryl isocyanide molecules with metal surfaces has been investigated in relation to spectral signals and bonding properties using spectroscopic methods such as near-edge X-ray absorption fine structure spectroscopy (NEXAFS) and temperature-dependent surface-enhanced Raman spectroscopy (SERS).[31]

Vibrational sum frequency generation (VSFG) spectroscopy is an intrinsically surface-specific detection technique.[32,33] Under the electric dipole approximation, SFG processes are intrinsically prohibited in media with inversion symmetry, but they can occur at the interface of two media where inversion symmetry is inevitably broken.[34] Thus, VSFG spectroscopy has been applied in many diverse fields, such as orientation anisotropy,[35] ultrafast direct electron transfer at the interface between organic semiconductors and metals,[36] observation of non-uniform charge distribution,[37] and cyanide-induced metal surface restructuring,[38–41] because it has unique surface properties and can provide new insights into the chemical properties of adsorbed species on metal substrates that cannot be obtained by conventional techniques such as Fourier transform infrared (FTIR) spectroscopy.

Quantum chemical calculations can also be used to explore the adsorption conformational changes of structurally well-defined SAMs on metal substrates, providing an intuitive and clear picture of the chemical bonding interactions between SAMs and surfaces at the molecular level. Charge transport between the adsorbed molecules and metal substrates is an important factor for interaction at the interface. Natural bond orbital (NBO) analysis transforms the electronic wavefunction into a representation based on a localized basis, and assigns the delocalized multi-electron wavefunction and electron pairs to one-center-two-electron orbitals (lone pairs) and two-center-two-electron bond, allowing us to analyze the bonding modes of molecular systems based on the wave function.[42] This NBO analysis has recently been extended to periodic systems and implemented in the Periodic NBO software[43] which has been used for determining the CO adsorption site preference on Pt(111) surface[44] and describing the bonding nature of transition state complex during CH_4 activation on TiO_2(110) surface.[45] We have investigated the NC bond strength of X−C_6H_4−NC molecules on a platinum surface using periodic-boundary density

functional theory (DFT) calculations with periodic NBO analysis, concentrating on the substituent effect.[22] The "volcano-like" trend of isolated molecules was considerably changed for molecule adsorbed on the Pt surface when the NC stretching frequencies and bond order derived by NBO analysis were plotted as a function of Hammett constant[46,47] for substituent X. This study shows that NBO analysis of the chemical bonds of various organic molecules adsorbed on a surface can provide a deeper understanding of the interaction between molecules and the surface.

The influence of substrate on adsorbed molecules has received a lot of attention. Experimental studies of biphenyl-based thiols on Au(111) and Ag(111) surfaces have revealed that these two surfaces have opposite odd-even effects, exhibiting a dependence on the orientation of the biphenyl moiety and the number of methylene groups.[48] Furthermore, studies of photoinduced electron dynamics at the interface of porphyrin on the Ag(111) and Ag(100) have shown that different substrate orientations cause differences in the energy alignments of the electronic states of the adsorbed molecules relative to the Fermi level of the metal surface, which dominate both static and photoinduced electron transfer processes.[49]

In this study, we aim to clarify the influence of the metal substrate on the spectral behavior in terms of the nature of chemical bonding between the molecule and the surface. The molecular vibrations and electronic wavefunctions of aryl isocyanide molecules adsorbed on Au(111) or Ag(111) substrate were chosen as target systems and investigated using experimental VSFG spectroscopy and theoretical calculations.

2. Experimental and Computational Methods

2.1. Experimental Setup

Glass slides (1.3 × 1.0 cm^2) were first cleaned in piranha solution (H_2SO_4/H_2O_2 = 3/1 v/v), rinsed copiously in Milli-Q water and dried under nitrogen blow. A 10 nm thick Ti film was evaporated onto the glass slides by a vacuum evaporator apparatus (ULVAC, EBH-6) under 2×10^{-6} Torr (monitored by ULVAC, GI-TL3) as an adhesion layer, followed by deposition of 100−150 nm gold and silver layers. Au (Tanaka Precious Metals) or Ag (Nilaco) wires (φ = 0.1 mm) were wound around a spiral bundle of three tungsten wires (Nilaco) that act as a support heater. These tungsten wires were cleaned in dichloromethane by ultrasonication prior to the preparation. The temperature of the substrate during gold and silver deposition was controlled by a hot plate controller (Chino Co., DB1000) at 300 ℃. The deposition rate and the thickness of films were measured by a quartz crystal thickness monitor (ULVAC, CRTM-5000). The deposition was carried out at the constant rate of 0.1 nm/s. The deposition rate was controlled by changing the current passed through the tungsten wires around which Au and Ag wires were wound. The samples were then cooled with pure N_2 put into the evaporator, taken out of the evaporator, and kept in hexane (Wako Pure Chemicals) after the evaporation. The Au films were annealed in a hydrogen flame for few seconds before immersing into the SAM formation solution. This method has been widely used for preparing the metal substrate, and the STM measurements have confirmed the predominance of (111) plane in films formed by this preparation procedure.[50−54]

Phenylisocyanide ($H-C_6H_4-NC$) (ABCR), 4-methoxyphenylisocyanide ($OCH_3-C_6H_4-NC$) (Sigma-Aldrich), and 4-nitrophenylisocyanide ($NO_2-C_6H_4-NC$) (Zerenex) were used without further purification. 10 mM solutions of aryl isocyanides were prepared by using dehydrated stabilizer free tetrahydrofuran (THF) (Kanto Chemical) as the solvent in an Ar(99.999%) purged

glove box. The Au and Ag thin films prepared by vapor deposition were then immersed in the isocyanide solutions for 48 hours in the glove box for depositing isocyanides on Au and Ag films to form SAMs. After the formation of isocyanide SAMs, Au and Ag substrates were rinsed with THF solution, and dried in a stream of N_2. During the preparation of solutions and immersion of the metal substrates, the oxygen concentration in the glove box was kept at 0.1−0.2 ppm and the dew-point temperature was kept below the lower limit of a hygrometer, i.e., below −100 ℃.

The 1 kHz femtosecond broad-band SFG (BB-SFG) system was used in this study. A detailed setup schematic of the system has been presented in our previous publication.[21] In brief, the loosely focused ps narrow-band visible (7 ps, ~8cm^{-1}) and broad-bandwidth IR (140 fs, ~200 cm^{-1}) beams were overlapped at the sample surface with incident angles of roughly 70 and 50 degrees, respectively. A spectrograph (Oriel Instruments, MS-257) equipped with an ICCD multi-channel detector (Andor technology, *i*Star, Model DH720-18F-13) was used to detect the SF light generated from the sample surface. The SFG spectrum was then obtained by dividing the ICCD output of the sample by that of bare Au. The temporal and spatial overlaps were adjusted by monitoring the SFG signal from a quartz plate. In this study, all spectra were collected using the p−p−p (SFG-visible-infrared) polarization combination. The SFG measurements were carried out at room temperature.

In SFG experiment, the intensity of the generated signal (I_{SFG}) is proportional to the square of the second-order nonlinear susceptibility $\chi^{(2)}$ as well as the visible and IR intensities:

$$I_{\mathrm{SFG}} \propto \left|\chi^{(2)}\right|^2 I_{\mathrm{vis}} I_{\mathrm{IR}} \qquad (1)$$

$\chi^{(2)}$ can be expressed as the coherent sum of a resonant part and a non-resonant part. As for the resonant part of susceptibility in the observed SFG spectra, we can expand $\chi^{(2)}$ as follows if we employ a Lorentzian line shape to account for the broadening:

$$\chi^{(2)} = \chi_{\mathrm{R}}^{(2)} + \chi_{\mathrm{NR}}^{(2)} = \frac{A}{\omega_{\mathrm{IR}} - \omega + i\Gamma}\exp(i\phi) + \chi_{\mathrm{NR}}^{(2)} \qquad (2)$$

where $\chi_{\mathrm{R}}^{(2)}$ is the vibrationally resonant mode summed over the available infrared bandwidth and $\chi_{\mathrm{NR}}^{(2)}$ represents the nonresonant electronic response from the surface itself (*e.g.* electronic transitions in Au(111) and Ag(111) surfaces and in isocyanide molecules). ω_{IR} is the frequency of the infrared pulse, and ω, A, ϕ, and Γ are the resonant frequency, transition amplitude, phase difference between $\chi_{\mathrm{R}}^{(2)}$ and $\chi_{\mathrm{NR}}^{(2)}$ responses of the system, and damping coefficient of the vibrational mode, respectively. The FTIR spectroscopy measurements were conducted to obtain the spectra of free aryl isocyanide molecules. The FTS-30 FTIR spectrometer (Bio-Rad) equipped with a DTGS detector was used to measure the FTIR of 10 mM hexane (Wako Pure Chemicals) solutions containing isocyanides. A spectrum with a resolution of 2 cm^{-1} resolution was created by combining 64 interferograms.

2.2. Computational Details

DFT calculations with spin-polarization scheme were carried out for aryl isocyanide molecules with different para-substituents X−C_6H_4−NC (X = H; NO_2 (electron-donating group); OCH_3 (electron-withdrawing group)) adsorbed on Au(111) and Ag(111) surfaces using VASP (Vienna Ab initio Simulation Package) software.[55−58] The Perdew-Burke-Ernzerhof functional in general gradient approximation (GGA-PBE)[59,60] was chosen as the XC functional, and the van der Waals interaction was taken into account in geometry optimization using the D3 energy correction with zero damping.[61] The core electrons are described by the projector-augmented wave method.[62,63] A plane-wave basis set with a kinetic energy cutoff of 540 eV was adopted for all calculations. Integration of the Brillouin zone was performed using the Methfessel−Paxton method[64] and a 9 × 9 × 1 mesh *k* grid centered at the Γ-point generated according to the Monkhorst–Pack scheme.[65] All structures were fully relaxed with a range of convergence of less than 10^{-6} eV in total energy and less than 0.02 eV/Å in force. The optimized lattice constants for bulk Au and Ag were 4.098 and 4.071 Å, respectively, in good agreement with the experimental values of 4.08 and 4.09 Å, respectively.[66] Using these equilibrium lattice constants, the Au(111) and Ag(111) surfaces were modeled as a structure with four layers of repeated slabs. The periodically repeated slabs are separated by a vacuum gap of 15 Å. The aromatic molecules and the top two metal layers were allowed to relax during geometry relaxation. The bottom two layers were fixed in their bulk-truncated positions using the optimized lattice constants of the bulk metals. Otherwise, the surfaces of both Au(111) and Ag(111) would not be reconstructed.

Based on the Hessian matrix and Born effective charge calculated using density functional perturbation theory (DFPT),[67,68] the vibrational spectra of aryl isocyanide molecule in the gas phase and on a metal substrate have been theoretically reproduced. The DFPT based method can

provide theoretical IR vibrational spectra of materials adsorbed on metal surfaces.[69–71] An anharmonic correction is applied to each vibrational mode by calculating the Morse-potential using the analytical method proposed by Torres *et. al.*[72]

In order to quantitatively analyze the chemical bonding of molecules adsorbed on the surface, periodic NBO calculations were performed to analyze the orbital occupancy and generate a visualization file. The plane-wave wavefunction obtained from static calculations using VASP was projected onto a Gaussian basis set from the EMSL basis set library.[73] For this purpose, we have selected the jorge-DZP basis set.[74–77] The evaluation of the C−N and C−metal interactions has been further conducted by chemical bonding analysis based on the Crystal Orbital Hamilton Population (COHP) implemented in the LOBSTER package.[78–82] Visualization for Electronic and Structural Analysis software (VESTA) was used to visualize the orbitals.[83]

3. Results and Discussion

3.1. VSFG and theoretical IR spectra of SAMs on Au(111) and Ag(111) surfaces

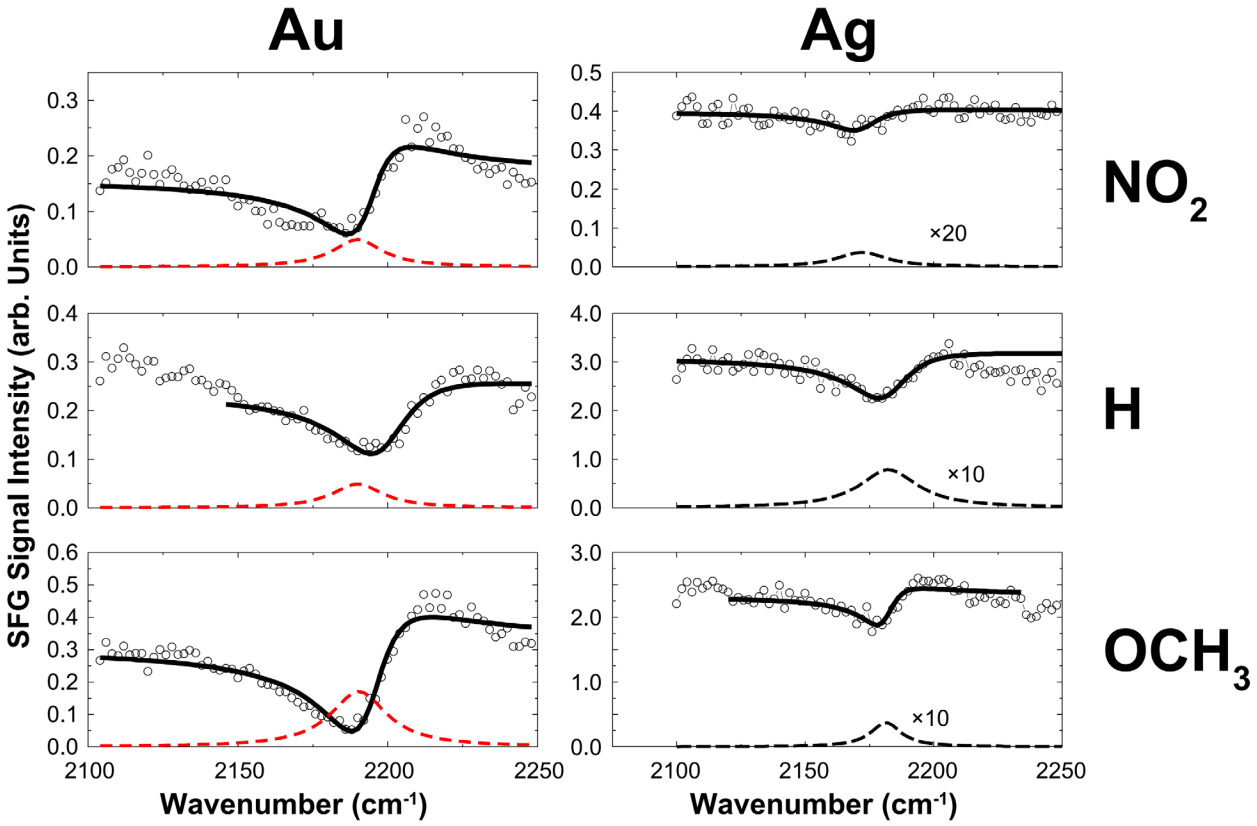

Figure 1. VSFG spectra in p–p–p polarization combination of NO_2–C_6H_4–NC, H–C_6H_4–NC, and OCH_3–C_6H_4–NC adsorbed on Au and Ag surfaces in the NC stretching region. The solid line shows the calculated fit to the VSFG data by eqn (2). The broken line corresponds to the resonance component when considering the sign of the resonant susceptibility $\chi_R^{(2)}$.

Figure 1 shows the VSFG spectra of three selected SAMs on Au and Ag surfaces, respectively. The non-resonant SFG signal of NO_2–C_6H_4–NC was lower than that of the other two molecules; the solvent of NO_2–C_6H_4–NC was yellow, which was due to the nitrophenol group. Due to this

strong visible light absorption, we speculate that NO_2−C_6H_4−NC has a weak background signal, which is observed when the strong non-resonant signal from the molecule and the non-resonant signal from the substrate interfere with each other. The spectra are fitted with the standard SFG spectral fitting formula (eqn (2)), and the fitting parameters are displayed in Table S1. The spectra are dominated by a single peak around 2180−2195 cm^{-1} in the frequency range, which is contributed by the NC stretching vibration and this spectral feature is assigned to on-top adsorption configuration when compared with previous literature.[21] The blue shift phenomenon is observed for SAMs adsorbed on Au and Ag surfaces with respect to the free isocyanide molecules measured by FTIR spectroscopy (Figure S1). For instance, FTIR measurements show that the NC stretching frequency of free molecule appears at around 2120 cm^{-1}, increasing to roughly 2195 cm^{-1} for SAMs−Au, and around 2180 cm^{-1} for SAMs−Ag. Thus, adsorbing on Au surface gives rise to a more significant blue shift than adsorbing on Ag surface.

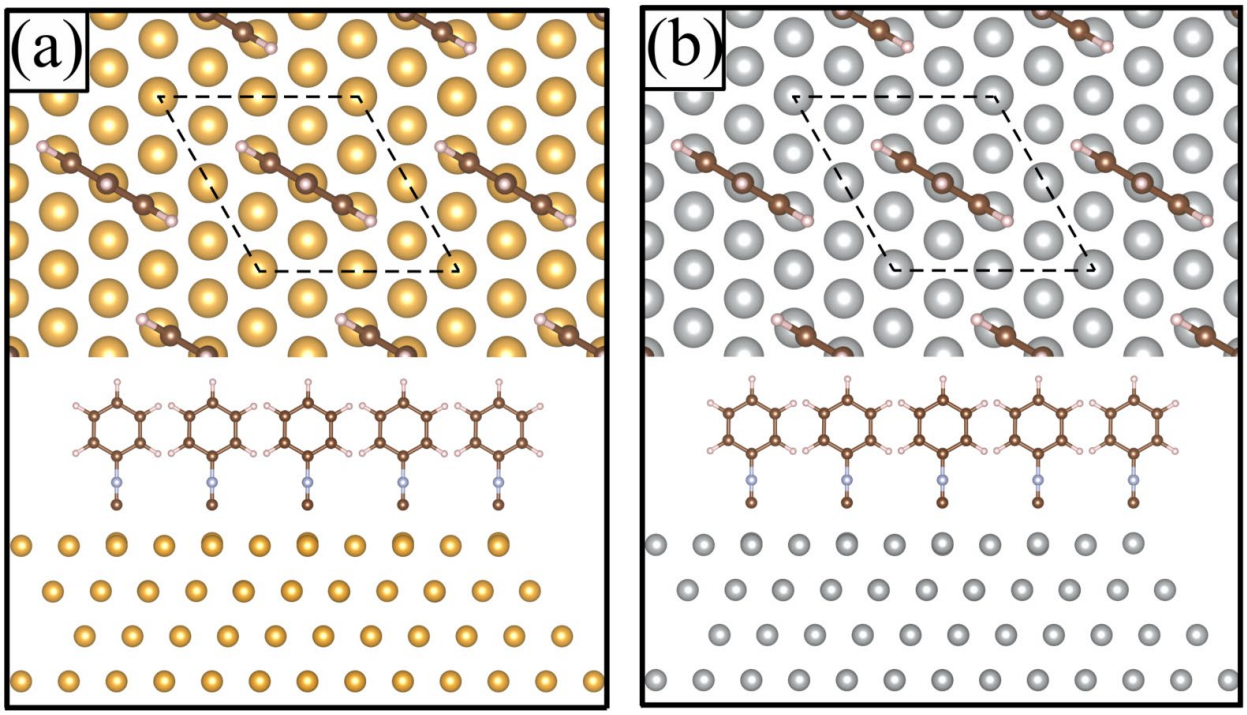

Figure 2. Top and side views of optimized H−C_6H_4−NC molecules adsorbed on (a) Au(111) and (b) Ag(111) surfaces. Gold, silver, gray, brown and red spheres represent Au, Ag, N, C and H atoms, respectively. Dash lines indicate the supercell used in this calculation.

As a next step, we calculated the theoretical IR vibrational spectra of SAMs adsorbed on Au and Ag surfaces starting from introduction of structural models. **Figure 2** shows the top and side views of the optimized H−C_6H_4−NC molecules adsorbed on (a) Au(111) and (b) Ag(111) surfaces. The H−C_6H_4−NC molecules perpendicularly adsorb on the metal surface which is similar with our previous results.[22] The N−C bond lengths and metal−C interatomic distances were summarized in **Table 1**. The N−C bond lengths show the same value for three free molecules, while they become slightly shorter for molecule adsorbed on Au and Ag surfaces. The distance between the adsorbed molecule and the metal surface is slightly shorter (< 0.1 Å) for the Au surface than for the Ag surface.

Table 1. N−C bond lengths (*r*(N−C)) and metal−C interatomic distances (*r*(metal−C)) calculated for NO_2−C_6H_4−NC, H−C_6H_4−NC, and OCH_3−C_6H_4−NC as free molecules and those adsorbed on Au(111) or Ag(111) surface.

		free	**Au**	**Ag**
NO_2−C_6H_4−NC	*r*(N−C)/Å	1.184	1.176	1.178
	r(metal−C)/Å	-	2.011	2.114
H−C_6H_4−NC	*r*(N−C)/Å	1.184	1.176	1.178
	r(metal−C)/Å	-	2.012	2.115
OCH_3−C_6H_4−NC	*r*(N−C)/Å	1.184	1.176	1.179
	r(metal−C)/Å	-	2.016	2.120

The adsorption energies estimated for X−C_6H_4−NC (X = NO_2, H, OCH_3) adsorbed on atop, bridge, and hollow sites on Au(111) and Ag(111) surfaces using the equation, $E_{ads} = E_{adsorbate@(surface)} - E_{adsorbate} - E_{(surface)}$, are shown in **Figure 3**. The results show that (1) the

adsorption energies for bridge and hollow adsorption sites are similar and are greater than that for top adsorption site, (2) no substitution (−H) molecule has a greater adsorption energy than molecules substituted with electron donating or electron withdrawing groups for both Au and Ag surfaces, and (3) the adsorption energy to the Au surface is stronger than to the Ag surface for all adsorbates. The inconsistent between experimental and theoretical results is due to the inaccuracy of GGA-based approach as discussed in Ref [*J. Phys. Chem. B* **2001**, *105* (18), 4018−4025]. Since our goal is to reveal the frequency-metal substrate dependence, we assume that the on-top site obtained experimentally is the direct adsorption site in our calculations.

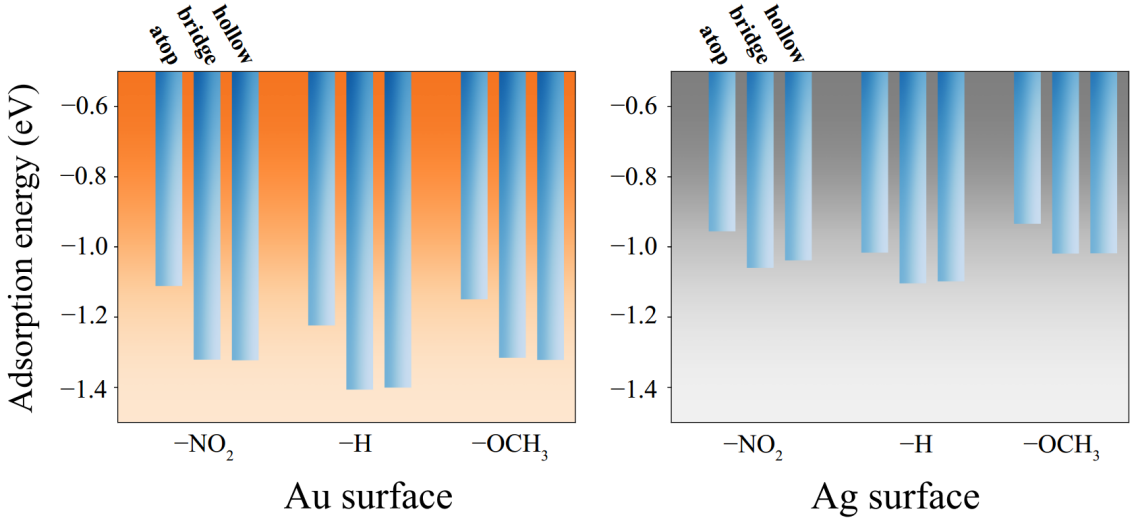

Figure 3. Adsorption energies of X−C_6H_4−NC (X = NO_2, H, OCH_3) adsorbed on atop, bridge and hollow sites of Au(111) and Ag(111) surfaces, respectively.

Figure 4 depicts the theoretical IR vibrational spectra of three isolated molecules and the molecules adsorbed on the Au and Ag surfaces. Calculation gives the largest relative intensity for isolated H−C_6H_4−NC molecule and H−C_6H_4−NC adsorbed on Au and Ag surfaces, in comparison to the NO_2−C_6H_4−NC and OCH_3−C_6H_4−NC derivatives. Since the intensity of the SFG spectra is proportional to the square of the second-order nonlinear susceptibility as well as

the visible and IR intensities as shown in eqn (1), it is difficult to make a direct comparison of the intensity between the experimental SFG spectra and theoretical IR spectra, and thus, we compare only the vibrational frequency between VSFG and theoretical spectra for isolated molecules and those adsorbed on Au and Ag surface. In analogy to the FTIR spectroscopy given in Fig. S1 in SI, the peaks centered at 2125 cm^{-1} (*para*-substituted $-NO_2$), 2133 cm^{-1} (unsubstituted) and 2131 cm^{-1} (*para*-substituted $-OCH_3$) of the isolated molecule are ascribed to the NC stretching frequency (ν_{NC}). The multiple peaks at 3000~3100 cm^{-1} belong to the stretching vibration of C−H bonds of OCH_3 group and C−H bond of aromatic ring (ν_{CH}). Additionally, symmetric and asymmetric stretching of the C−C bond of the aromatic ring appears around 1500 cm^{-1}, and the vibration frequency identified around 1000 cm^{-1} is attributed to the C−H in-plane bending mode. Since the goal of this study is to clarify the effect of the metal substrate on the interfacial structure, subsequent discussions will focus on the N−C bond stretching vibration, which is directly involved in the adsorption of molecules to the metal surface.

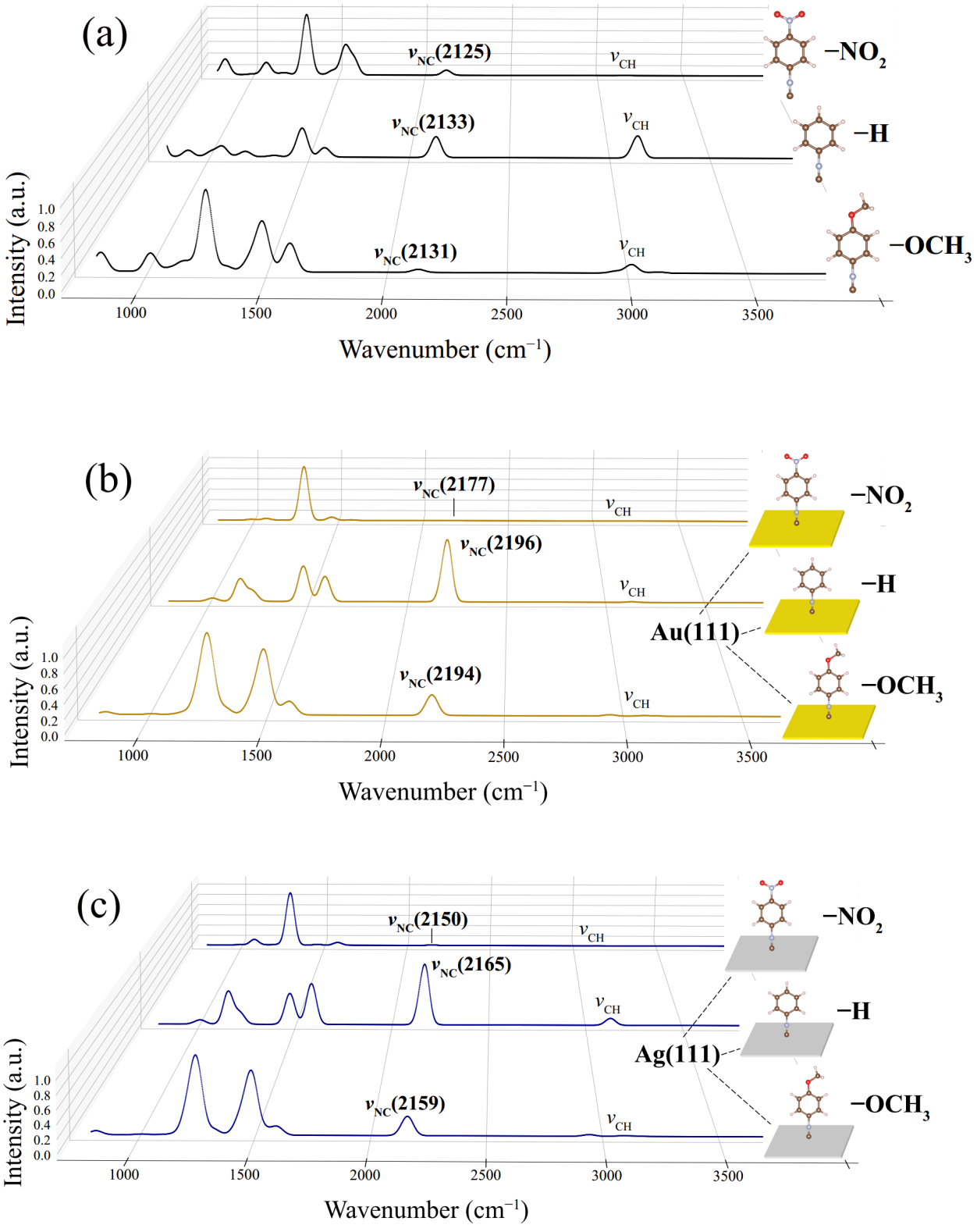

Figure 4. Calculated vibrational spectra of X−C_6H_4−NC molecule (X = NO_2, H, OCH_3) (a) without substrate, (b) on the Au(111) surface, and (c) on the Ag(111) surface.

After adsorption, the NC stretching frequency on Au and Ag surfaces exhibits a blue shift when compared to that of isolated molecules, as shown in Figures 4b and 4c, respectively. Importantly, Au surface exhibits a larger blue shift than the Ag surface (50~60 cm^{-1} vs. 30~40 cm^{-1}). This blue shift occurrence in the spectrum is also confirmed by VSFG spectroscopy measurements presented in previous section.

Table 2. NC stretching frequencies of free $X{-}C_6H_4{-}NC$ molecule ($X = NO_2$, H, OCH_3) in dilute hexane solution obtained by FTIR spectroscopy, and NC stretching frequencies of molecules adsorbed on Au or Ag surface obtained by VSFG spectroscopy. Calculated anharmonic frequencies by DFPT method are also given. The unit of frequency is cm^{-1}.

	experiment			calculation		
X	free (FTIR)	Au (SFG)	Ag (SFG)	free	Au	Ag
$-NO_2$	2119	2194	2176	2125	2177	2150
−H	2123	2199	2186	2133	2196	2165
$-OCH_3$	2122	2194	2185	2131	2194	2159

The experimental and calculated NC stretching vibrational frequencies were summarized and compared in **Table 2**. The calculated frequencies for isolated molecules are quite close to the FTIR spectroscopy experimental results. The unsubstituted molecule possess the largest frequencies irrelevant to the metal support. Also, NC stretching frequencies on metal support is in an order of free molecule < Ag < Au for all the substituted groups. This indicates that our computational model and the DFPT method are both capable of accurately describing the experimental vibrational frequencies. Moreover, it was noticed that relationship between bond length and bond strength (vibrational frequency) is not applicable in the current systems. An in-depth understanding in the electronic structure of SAMs/substrate interfaces is therefore necessary.

3.2. Electronic Structure of X−C_6H_4−NC/substrate interfaces

To clarify the mechanism behind the effect of the metal substrate on the vibrational spectrum, the electronic structure of the SAMs/substrate interface was analyzed. First, the density of states (DOS) was calculated to investigate how the electronic state of the aryl isocyanide molecule is redistributed upon interaction with the adsorbed metal substrate. Furthermore, by projecting the overall DOS onto the atomic orbitals (PDOS), the contributions from the individual atoms were assigned. For clarity, only NC groups rather than all atoms in the adsorbed molecule are plotted, and atomic orbitals with a contribution of less than 2% to the overall DOS are ignored. **Figure 5** shows the PDOS of the NC group of an isolated H−C_6H_4−NC molecule, clean Au and Ag surfaces, and the NC group of H−C_6H_4−NC molecules adsorbed on Au and Ag surfaces, respectively. Figure 5a indicates that the density of NC groups in the isolated molecules is discrete; the C 2s and C 2p orbitals contribute to the 5σ orbital of the N−C bond, while the C 2p and N 2p form a 2π* orbital at 6 eV above the Fermi level (E_F). Figures 5b and 5c show the PDOS of clean Au and Ag surfaces before adsorption, showing a sharp drop from E_F to −2 eV for Au and around −3 eV for Ag. The d states of Au and Ag are mainly located in the range of −6 to −2 eV and −7 to −3 eV, respectively; the contributions of the s and p states of Au and Ag are comparable to those of the d states in the vicinity of E_F. This delocalized s, p, and d states suggest a hybridization of d and sp states at clean metal surfaces.

As shown in Figure 5d, the PDOS of the H−C_6H_4−NC molecule is significantly changed by adsorption on the metal surface. First, the C 2p state of adsorbed H−C_6H_4−NC is resonantly broadened and shifts to lower energies towards the bottom of the Au valence state. This is due to the strong interaction between the 5σ (a hybridized state of C 2s and 2p) and the metal d state, which forms a localized state around the bottom of the Au valence state. This means that,

electron donation from the 5σ orbital of the adsorbate to the Au d state has occurred which is called the σ donation process. In addition, resonance state with antibonding character (5σ-d antibonding state) is formed and located close to E_F. On the other hand, the 1π state of NC group interacts with the d orbitals of Au. Due to the strong σ interaction, this state (1π-d) now lies above the 5σ-d localized state, and the interaction between the 1π and d states splits into two peaks with energies around −6.4 eV and −3.4 eV, can be assigned to bonding and antibonding contributions, respectively, as illustrated by the COHP analysis in Figure S2 in SI. The 1π-d bonding combination is a localized state near the bottom of the Au valence state. On the other hand, the 1π-d antibonding combination resonates with the d state. 2π*-d interaction also results in one bonding combination near E_F and another antibonding state appearing at about 3 eV above E_F, which is known as the π back-donation process. This PDOS is qualitatively similar to the previous literatures on 1,4-phenylenediisocyanide adsorbed on the Au(111) surface[84] and HNC adsorbed on the Au(111) surface.[85]

The PDOS of the NC group of the H−C_6H_4−NC molecule adsorbed on the Ag surface is almost the same as the PDOS of the Au surface, as shown in Figure 5e. The PDOS analysis indicates that the 5σ orbital of the NC bond donates electrons to the metal surface to form the Au/Ag−C bond, while the 2π* orbital of the NC accepts electrons through a back-donation from the Au/Ag d orbitals to weaken the NC bond.

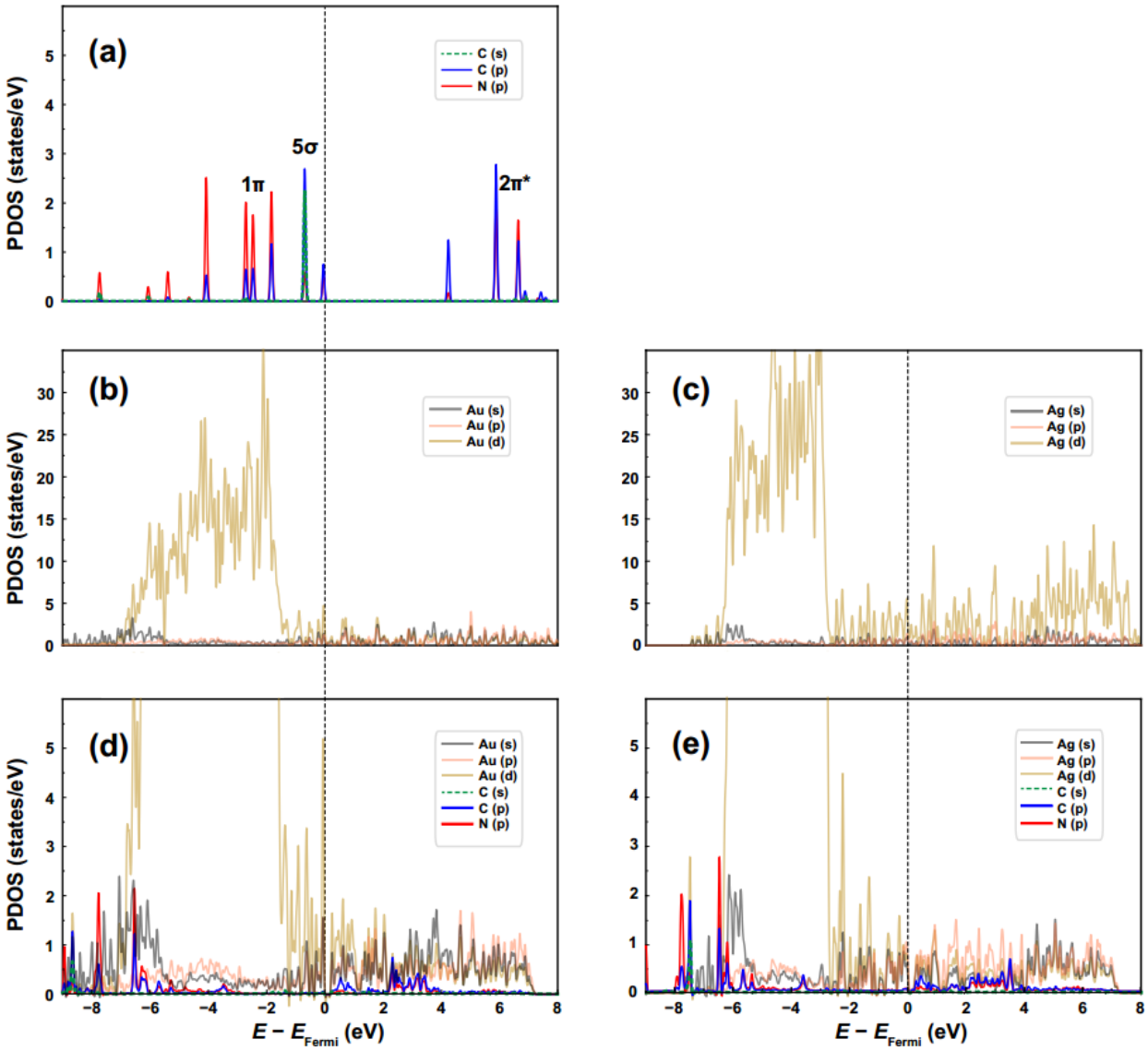

Figure 5. PDOS projected onto (a) NC group of a free H−C_6H_4−NC molecule, (b), (c) clean Au(111) and Ag(111) surfaces, and (d), (e) NC group of an H−C_6H_4−NC molecule adsorbed on Au(111) and Ag(111) surfaces. The Fermi level is indicated by the black dashed line located at 0 eV. Only the states accounting for more than 2% of the total DOS are considered.

Natural population analysis (NPA) was performed to evaluate the overall electron density distribution after adsorption, and the results are shown in **Table 3**. Upon binding to Au and Ag

surfaces, the fully localized lone pair on the isocyanide group is converted to shared metal−C bond, resulting in more positively charged isocyanide group. The amount of charge loss of the isocyanide group after binding to the Au surface is greater than after binding to Ag (0.250*e* versus 0.188*e*). This difference emphasizes the effect of the metal support and may be related to the strength of the σ donation/π back-donation discussed below.

Table 3. Results of natural population analysis for H−C_6H_4−NC molecule adsorbed on Au(111) and Ag(111) surfaces. For comparison, natural charges for isolated molecules and clean metal surfaces are also listed.

H−C_6H_4−NC on Au(111) surface			
	Au	C	N
before adsorption/*e*	+0.072	+0.259	−0.490
after adsorption/*e*	−0.353	+0.393	−0.374
H−C_6H_4−NC on Ag(111) surface			
	Ag	C	N
before adsorption/*e*	+0.095	+0.259	−0.490
after adsorption/*e*	−0.269	+0.343	−0.386

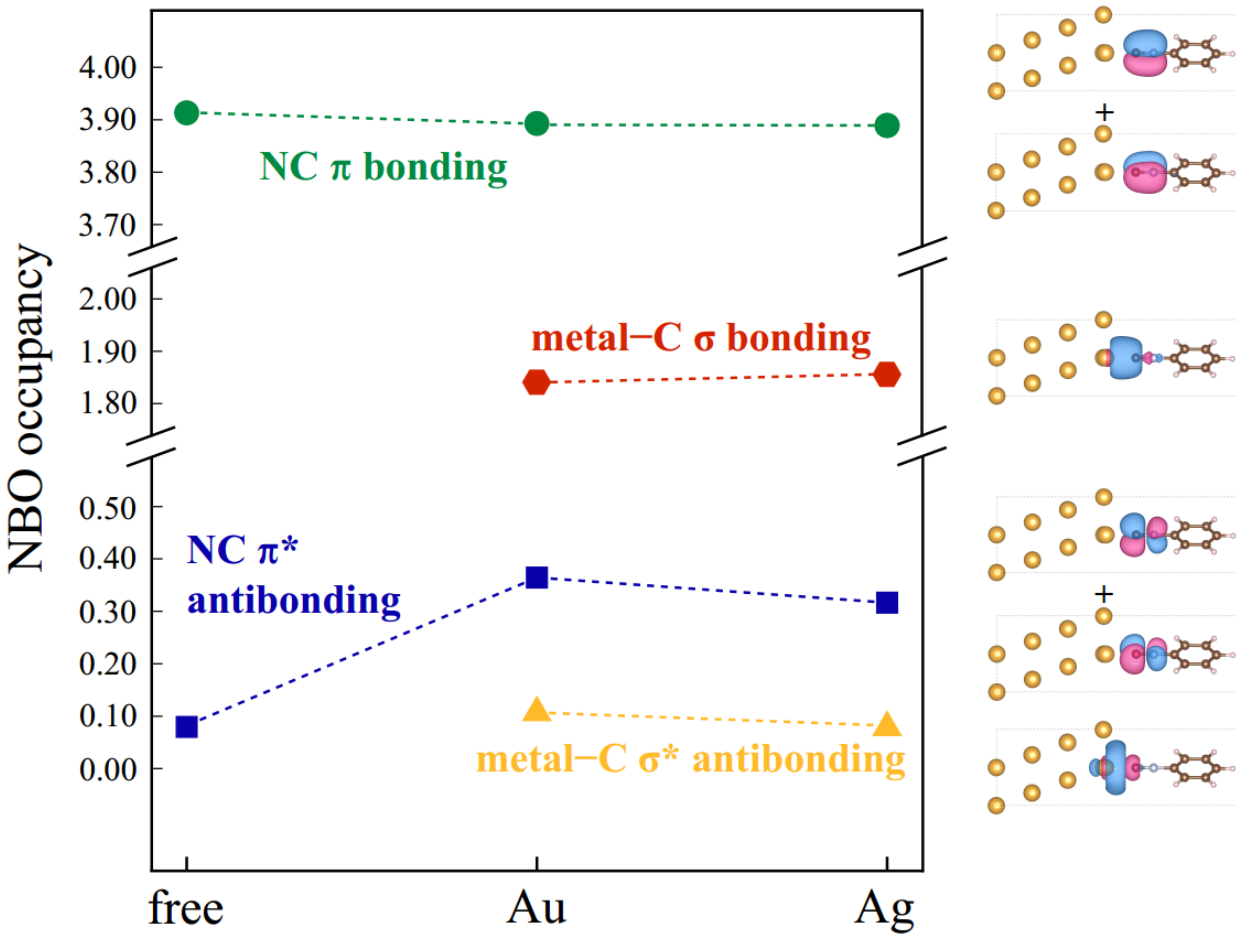

Figure 6. NBO occupancy of NC π bonding orbitals, metal−C σ bonding orbitals, NC π* antibonding orbitals, and metal−C σ* antibonding orbitals calculated for free H−C_6H_4−NC molecules and H−C_6H_4−NC molecules adsorbed on Au or Ag surfaces. The NBOs are featured in the right panel. An isosurface value of 0.035 *e*/Bohr^3 is used.

NBO algorithm implemented for periodic system was applied to quantitatively elucidate the surface chemical bonding interactions and gain a deeper understanding of the distinctions between Au and Ag surfaces. **Figure 6** shows the calculated NBO occupancies in several representative orbitals, including NC π bonding orbital, metal−C σ bonding orbital, NC π* antibonding orbital, and metal−C σ* antibonding orbital, for free H−C_6H_4−NC molecules and

molecules adsorbed on Au and Ag surfaces, respectively. The occupancy of NC π bonding orbitals (green dots) in free molecule (3.92*e*) and molecules adsorbed on the metal support (3.89*e* for Au and Ag) suggests that the NC bonding orbitals were somewhat involved in the formation of chemical bonds between molecules and surfaces, but the equal decrease for Au and Ag indicates that NC bonding orbital is not sensitive to changes in the metal substrate. The red dots show the metal−C σ bonding orbital formed by σ donation. It was shown that metal−C bond orbitals are virtually double occupied in Au and Ag cases with occupancies of 1.84*e* and 1.86*e*, respectively.

According to the σ-donation−π* back-donation mechanism, filled 5σ and empty 2π* orbitals of unbound NC group first couple with the sp states of Au and Ag, then the coupled states further hybridize with the d states of Au and Ag. Among the generated hybridized states, the metal−C σ* antibonding and NC π* antibonding orbitals are responsible for σ donation and π* back-donation, respectively.[23] As such, their occupancy can be used as a suitable indicator of the donation and back-donation strengths. The blue dots represent the NBO occupancy in NC π* states. The fact that Au has a higher occupancy (0.36*e*) than Ag (0.32*e*) indicates that Au has a greater π* back-donation strength. Due to the antibonding nature of π* orbital, π* back-donation weakens the NC bond strength, causing a red shift of NC stretching vibration.

On the other hand, Au−C σ* orbital has a higher occupancy (0.11*e*) than Ag−C σ* orbital (0.08*e*), as indicated by yellow dots in Figure 6, implying a greater σ donation strength for Au substrate. Since the 5σ orbital of NC bond has a weak antibonding character which will be suppressed during σ donation process and formation of metal−C adsorption bond, resulting in an enhanced NC bonding and a blue shift in the NC stretching frequency.[86] This blue shift effect is more pronounced for Au than Ag.

In addition to these essential states, NC σ bonding orbital and σ* antibonding orbital have also been studied, as listed in Table S2. In comparison to unbound NC group, only tiny changes ($\Delta<0.01e$) have been found after binding to Au and Ag surfaces. The essentially unperturbed occupancies in NC σ bonding orbital confirms again that the adsorption bond at the SAMs/metal substrate interface is formed mainly from the 5σ orbital of the unbound NC group, with a relatively minor contribution from the NC π bonding orbital.

To confirm the presence of metal substrate-induced NBO occupancy changes for other adsorbates, NBO analysis was also performed for two other derivatives (NO_2−C_6H_4−NC and OCH_3−C_6H_4−NC), as shown in Table S3. The results show that the σ donation on the Au surface is stronger than on the Ag surface when the −H is replaced with a different group. Moreover, different basis set combinations have been used for projection, and the results of some typical orbitals are shown in Table S4. The results show that increasing the size of basis set does not improve the quality of the results, and a double-ζ basis set seems to be sufficient for the projection work in this study. We also found a good linear relationship between an adsorption energy and NBO occupancy in metal−C σ* antibonding orbital (named as 5σ-d antibonding orbital in PDOS and -COHP analysis) for adsorptions on atop site of Au and Ag surfaces as shown in **Figure S4** in SI**.** The adsorption energy becomes larger as the NBO occupancy in metal−C σ* antibonding orbital increases, indicating that the NBO occupancy is a good descriptor for predicting an adsorption energy.

In summary, we can conclude that no matter the substituent group, SAMs on the Au surface have both stronger σ donation and π* back-donation than SAMs on the Ag surface. For both Au and Ag, the overall blue shift of the NC stretching frequency after binding to the metal surface is due to a stronger involvement of σ donation than π* back-donation, based on the VSFG spectra

together with the results of calculation. More crucially, the stronger σ donation for the Au surface results in a greater blue shift in frequency than the Ag surface, demonstrating the impact of the metal substrate on chemical bonding nature at the interfacial area.

4. Conclusion

We have investigated the metal substrate-dependent chemical bonding nature of aryl isocyanide molecules (SAMs) adsorbed on two typical metal surfaces, Au(111) and Ag(111), with combining experimental VSFG spectra and theoretical calculations. The self-assembly molecular systems were constructed by immersing the Au(111) and Ag(111) thin films prepared by vapor deposition in isocyanide solution. The fabricated structures were well characterized by surface-specific VSFG spectroscopy. Compared to isolated aryl isocyanide molecules, the NC stretching frequency shows a blue shift on metal supports, and the blue shift is more evident with the Au(111) than one with Ag(111) substrate. In order to understand the experimental results rationally, we carried out theoretical calculations using density functional perturbation theory and the natural bond orbital approach adopted for periodic systems. The calculated trend for NC stretching frequency is well consistent with the experimental results. The ability of metal−C σ donation is the decisive factor for blue shift of NC vibration frequencies. Compared to Ag surface, the stronger σ donation from Au−C σ* antibonding orbital makes larger blue shift in NC vibrational frequencies. This study provides systematic insights into the relationship between vibrational frequency and natural orbital population, as well as suggestions for designing molecule/metal interfaces with desirable electronic properties using a variety of metal substrates.

Associated Content

Supporting Information

Parameters for fitting the VSFG spectra shown in Figure 1 (Table S1); Results of FTIR spectroscopy measurement for isolated $NO_2{-}C_6H_4{-}NC$, $H{-}C_6H_4{-}NC$, and $OCH_3{-}C_6H_4{-}NC$ molecules (Figure S1); −pCOHP plots for free $H{-}C_6H_4{-}NC$ molecule and $H{-}C_6H_4{-}NC$ molecule adsorbed on Au surface (Figure S2); NBOs of isolated $H{-}C_6H_4{-}NC$ molecule (Figure S3); NBO occupancies of NC σ bonding and NC σ* antibonding orbitals calculated for isolated $H{-}C_6H_4{-}NC$ molecule and $H{-}C_6H_4{-}NC$ molecule adsorbed on Au(111) or Ag(111) surfaces (Table S2); NBO occupancy analysis conducted for $NO_2{-}C_6H_4{-}NC$, $OCH_3{-}C_6H_4{-}NC$ derivatives (Table S3); NBO occupancies in some typical orbitals when projecting on various basis set combinations (Table S4); Comparison between various charge models (Bader, NPA, Hirshfeld, and DDEC6) for $H{-}C_6H_4{-}NC$ on Au surface (Table S5); a relationship between an adsorption energy and NBO occupancy in metal−C σ* antibonding orbital for adsorptions on atop site of Au and Ag surfaces as shown in (Figure S4).

Author Information

Corresponding Authors

Kohei Uosaki – *Global Research Centre for Environment and Energy based on Nanomaterials Science (GREEN), National Institute for Materials Science (NIMS), Tsukuba 305-0044, Japan;* orcid.org/0000-0001-8886-3270; Email: uosaki.kohei@nims.go.jp

Tetsuya Taketsugu – *Department of Chemistry, Faculty of Science, Hokkaido University, Sapporo 060-0810, Japan; Institute for Chemical Reaction Design and Discovery (WPI-ICReDD), Hokkaido University, Sapporo 001-0021, Japan;* orcid.org/0000-0002-1337-6694; Email: take@sci.hokudai.ac.jp

Authors

Ben Wang – *Department of Chemistry, Faculty of Science, Hokkaido University, Sapporo 060-0810, Japan*

Mikio Ito − *Department of Chemical Science and Engineering, National Institute of Technology, Tokyo College, 1220-2 Kunugida-machi, Hachioji, Tokyo 193-0997, Japan*

Min Gao − *Institute for Catalysis, Hokkaido University, Sapporo 001-0021, Japan*

Hidenori Noguchi − *Center for Global Research on Energy and Environmental Materials (GREEN), National Institute for Materials Science (NIMS), Tsukuba 305-0044, Japan*

Author Contributions

The manuscript was written through contributions of all authors. All authors have given approval to the final version of the manuscript.

Notes

The authors declare no competing financial interest.

Acknowledgements

B.W. thanks the China Scholarship Council for his PhD fellowship (CSC student number 201808050073) and the MEXT Doctoral program for DataRelated InnoVation Expert Hokkaido University (D-DRIVE-HU). This work was also partly supported by the Elements Strategy Initiative of MEXT (JPMXP0112101003), the Photoexcitonix Project at Hokkaido University, and JST CREST, Japan (JPMJCR1902). We gratefully acknowledge the Center for Computational Materials Science, Institute for Materials Research, Tohoku University, for the use of MASAMUNE-IMR. A part of calculations was performed using the Research Center for Computational Science, Okazaki, Japan.

References

1. Ratner, M. A brief history of molecular electronics. *Nat. Nanotechnol.* **2013**, *8*, 378−381.
2. Sun, L.; Diaz-Fernandez, Y. A.; Gschneidtner, T. A.; Westerlund, F.; Lara-Avila, S.; Moth-Poulsen, K. Single-molecule electronics: from chemical design to functional devices. *Chem. Soc. Rev.* **2014**, *43*, 7378−7411.
3. Xiang, D.; Wang, X.; Jia, C.; Lee, T.; Guo, X. Molecular-Scale Electronics: From Concept to Function. *Chem. Rev.* **2016**, *116*, 4318−4440.
4. Jia, C.; Guo, X. Molecule−Electrode Interfaces in Molecular Electronic Devices. *Chem. Soc. Rev.* **2013**, *42*, 5642−5660.
5. Chadwick, H.; Beck, R. D. Quantum State Resolved Gas-Surface Reaction Dynamics Experiments: A Tutorial Review. *Chem. Soc. Rev.* **2016**, *45*, 3576−3594.
6. Deng, G.-H.; Qian, Y.; Rao, Y. Development of Ultrafast Broadband Electronic Sum Frequency Generation for Charge Dynamics at Surfaces and Interfaces. *J. Chem. Phys.* **2019**, *150*, 024708.
7. Saalfrank, P. Quantum Dynamical approach to ultrafast molecular desorption at surfaces. *Chem. Rev.* **2006**, *106*, 4116−4159.
8. Browne, W. R.; Feringa, B. L. Light Switching of Molecules on Surfaces. *Annu. Rev. Phys. Chem.* **2009**, *60*, 407−428.
9. Metzger, R. M. Unimolecular Electronics. *Chem. Rev.* **2015**, *115*, 5056−5115.
10. Vilan, A.; Cahen, D. Chemical Modification of Semiconductor Surfaces for Molecular Electronics. *Chem. Rev.* **2017**, 117, 4624−4666.

11. Love, J. C.; Estroff, L. A.; Kriebel, J. K.; Nuzzo, R. G.; Whitesides, G. M. Self-Assembled Monolayers of Thiolates on Metals as a Form of Nanotechnology. *Chem. Rev.* **2005**, *105*, 1103−1170.
12. Uosaki, K.; Kondo, T.; Zhang, X.-Q.; Yanagida, M. Very Efficient Visible-Light-Induced Uphill Electron Transfer at a Self-Assembled Monolayer with a Porphyrin−Ferrocene−Thiol Linked Molecule. *J. Am. Chem. Soc.* **1997**, *119*, 8367−8368.
13. Vericat, C.; Vela, M. E.; Benitez, G.; Carro, P.; Salvarezza, R. C. Self-Assembled Monolayers of Thiols and Dithiols on Gold: New Challenges for a Well-Known System. *Chem. Soc. Rev.* **2010**, *39*, 1805−1834.
14. de Melo Souza, A.; Rungger, I.; Pontes, R. B.; Rocha, A. R.; da Silva, A. J. R.; Schwingenschlöegl, U.; Sanvito, S. Stretching of BDT-Gold Molecular Junctions: Thiol or Thiolate Termination? *Nanoscale* **2014**, *6*, 14495−14507.
15. Horiguchi, K.; Tsutsui, M.; Kurokawa, S.; Sakai, A. Electron transmission characteristics of Au/1,4-benzenedithiol/Au junctions. *Nanotechnology*, **2009**, *20*, 025204.
16. Ikeda, K.; Suzuki, S.; Uosaki, K. Crystal Face Dependent Chemical Effects in Surface Enhanced Raman Scattering at Atomically Defined Gold Facets. *Nano Lett.* **2011**, *11*, 1716−1722.
17. Inagaki, M.; Motobayashi, K.; Ikeda, K. Electrochemical THz-SERS Observation of Thiol Monolayers on Au(111) and (100) Using Nanoparticle-assisted Gap-Mode Plasmon Excitation. *J. Phys. Chem. Lett.* **2017**, *8*, 4236−4240.
18. Ikeda, K.; Takeuchi, Y.; Kanamaru, K.; Suzuki, S.; Uosaki, K. Nanostructuring of Molecular Assembly Using Electrochemical Reductive Desorption of Locally Stabilized Thiol Monolayers. *J. Phys. Chem. C* **2016**, *120*, 15823−15829.

19. Kim, B.-S.; Beebe, J. M.; Jun, Y.; Zhu, X.-Y.; Frisbie, C. D. Correlation between HOMO Alignment and Contact Resistance in Molecular Junctions: Aromatic Thiols versus Aromatic Isocyanides. *J. Am. Chem. Soc.* **2006**, *128*, 4970−4971.
20. Kiguchi, M.; Miura, S.; Hara, K.; Sawamura, M.; Murakoshi, K. Conductance of a Single Molecule Anchored by an Isocyanide Substituent to Gold Electrodes. *Appl. Phys. Lett.* **2006**, *89*, 213104.
21. Ito, M.; Noguchi, H.; Ikeda, K.; Uosaki, K. Substrate Dependent Structure of Adsorbed Aryl Isocyanides Studied by Sum Frequency Generation (SFG) Spectroscopy. *Phys. Chem. Chem. Phys.* **2010**, *12*, 3156−3163.
22. Wang, B.; Gao, M.; Uosaki, K.; Taketsugu, T. A Quantum Chemical Study of Substituent Effects on CN Bonds in Aryl Isocyanide Molecules Adsorbed on the Pt Surface. *Phys. Chem. Chem. Phys.* **2020**, *22*, 12200−12208.
23. Hu, J.; Tanabe, M.; Sato, J.; Uosaki, K.; Ikeda, K. Effects of Atomic Geometry and Electronic Structure of Platinum Surfaces on Molecular Adsorbates Studied by Gap-Mode SERS. *J. Am. Chem. Soc.* **2014**, *136*, 10299−10307.
24. Hu, J.; Hoshi, N.; Uosaki, K.; Ikeda, K. Vibrational Spectroscopic Observation of Atomic-Scale Local Surface Sites Using Site-Selective Signal Enhancement. *Nano Lett.* **2015**, *15*, 7982−7986.
25. Ikeda, K.; Fujimoto, N.; Uosaki, K. Nanoscale Optical and Mechanical Manipulation of Molecular Alignment in Metal−Molecule−Metal Structures. *J. Phys. Chem. C* **2014**, *118*, 21550−21557.

26. Ikeda, K.; Sato, J.; Uosaki, K. Surface-enhanced Raman scattering at well-defined single crystalline faces of platinum-group metals induced by gap-mode plasmon excitation. *J. Photochem. Photobiol., A* **2011**, *221*, 175−180.
27. Ikeda, K.; Kimura, A.; Uosaki, K. Electrochemical SERS observation of molecular adsorbates on Ru/Pt-modified Au(111) surfaces using sphere-plane type gap-mode plasmon excitation. *J. Electroanal. Chem.* **2017**, *800*, 151−155.
28. Ikeda, K.; Sato, J.; Fujimoto, N.; Hayazawa, N.; Kawata, S.; Uosaki, K. Plasmonic Enhancement of Raman Scattering on Non-SERS-Active Platinum Substrates. *J. Phys. Chem. C* **2009**, *113*, 11816−11821.
29. Ikeda, K.; Fujimoto, N.; Uehara, H.; Uosaki, K. Raman Scattering of Aryl Isocyanide Monolayers on Atomically Flat Au(111) Single Crystal Surfaces Enhanced by Gap-Mode Plasmon Excitation. *Chem. Phys. Lett.* **2008**, *460*, 205−208.
30. Hu, W.; Duan, S.; Zhang, Y.; Ren, H.; Jiang, J.; Luo, Y. Identifying the structure of 4-chlorophenyl isocyanide adsorbed on Au(111) and Pt(111) surfaces by first-principles simulations of Raman spectra. *Phys. Chem. Chem. Phys.* **2017**, *19*, 32389−32397.
31. Kim, S.; Ihm, K.; Kang, T.-H.; Hwang, S.; Joo, S.-W. Binding property and structure of aromatic isocyanide self-assembly monolayers on Ag and Au surfaces. *Surf. Interface Anal.* **2005**, *37*, 294−299.
32. Shen, Y. R. The Principles of Nonlinear Optics; John Wiley & Sons: New York, 1984.
33. Nihonyanagi, S.; Mondal, J. A.; Yamaguchi, S.; Tahara, T. Structure and Dynamics of Interfacial Water Studied by Heterodyne-Detected Vibrational Sum-Frequency Generation. *Annu. Rev. Phys. Chem.* **2013**, *64*, 579.

34. Nihonyanagi, S.; Yamaguchi, S.; Tahara, T. Ultrafast Dynamics at Water Interfaces Studied by Vibrational Sum Frequency Generation Spectroscopy. *Chem. Rev.* **2017**, *117*, 10665−10693.

35. Tuladhar, A.; Chase, Z. A.; Baer, M. D.; Legg, B. A.; Tao, J. H.; Zhang, S.; Winkelman, A. D.; Wang, Z. M.; Mundy, C. J.; De Yoreo, J. J.; Wang, H. F. Direct Observation of the Orientational Anisotropy of Buried Hydroxyl Groups inside Muscovite Mica. *J. Am. Chem. Soc.* **2019**, *141*, 2135−2142.

36. Xiang, B.; Li, Y.; Pham, C. H.; Paesani, F.; Xiong, W. Ultrafast direct electron transfer at organic semiconductor and metal interfaces. *Sci. Adv.*, **2017**, *3*, e1701508.

37. Piontek, S. M.; DelloStritto, M.; Mandal, B.; Marshall, T.; Klein, M. L.; Borguet, E. Probing Heterogeneous Charge Distributions at the α-Al_2O_3(0001)/H_2O Interface. *J. Am. Chem. Soc.* **2020**, *142*, 12096−12105.

38. Ghalgaoui, A.; Doudin, N.; Calaza, F.; Surnev, S.; Sterrer, M. Ordered Au nanoparticle array on Au(111) through coverage control of precursor metal-organic chains. *J. Phys. Chem. C* **2016**, *120*, 17418−17426.

39. Ghalgaoui, A.; Doudin, N.; Sterrer, M. Nanostructuring of Au(111) during the adsorption of an aromatic isocyanide from solution. *Langmuir* **2017**, *33*, 91−99.

40. Ghalgaoui, A.; Doudin, N.; Kelderer, E.; Sterrer, M. 1,4-Phenylene Diisocyanide (PDI) Interaction with Low-Coordinated Gold Sites: Dissociation and Adsorbate-Induced Restructuring. *J. Phys. Chem. C* **2019**, *123*, 7870−7878.

41. Ghalgaoui, A.; Sterrer, M. Direct Spectroscopic Observation of Cyanide-Induced Restructuring of Pt at the Solid-Liquid Interface. *J. Phys. Chem. C* **2020**, *124*, 7, 4190−4195.

42. Weinhold, F. and Landis, C. *Valency and Bonding–A Natural Bond Orbital Donor-Acceptor Perspective*; Cambridge University Press: Cambridge, 2005; pp 1−44.
43. Dunnington, B. D.; Schmidt, J. R. Generalization of Natural Bond Orbital analysis to periodic Systems: Applications to solids and surfaces via plane-wave density functional theory. *J. Chem. Theory Comput.* **2012**, *8*, 1902−1911.
44. Kalhara Gunasooriya, G. T. K.; Saeys, M. CO Adsorption Site Preference on Platinum: Charge Is the Essence. *ACS Catal.* **2018**, *8*, 3770−3774.
45. Zhou, M.; Wang, H. Optimally Selecting Photo- and Electrocatalysis to Facilitate CH_4 Activation on TiO_2(110) Surface: Localized Photoexcitation versus Global Electric-Field Polarization. *JACS Au* **2022**, *2*, 188−196.
46. Hammett, L. P. The Effect of Structure Upon the Reactions of Organic Compounds. Benzene Derivatives. *J. Am. Chem. Soc.* **1937**, *59*, 96−103.
47. Hansch, C.; Leo, A.; Taft, R. A survey of Hammett substituent constants and resonance and field parameters. *Chem. Rev.* **1991**, *91*, 165−195.
48. Rong, H.-T.; Frey, S.; Yang, Y.-J.; Zharnikov, M.; Buck, M.; Wühn, M.; Wöll, C.; Helmchen, G. On the Importance of the Headgroup Substrate Bond in Thiol Monolayers: A Study of Biphenyl-Based Thiols on Gold and Silver. *Langmuir* **2001**, *17*, 1582−1593.
49. Tognolini, S.; Ponzoni, S.; Sedona, F.; Sambi, M.; Pagliara, S. Role of the Substrate Orientation in the Photoinduced Electron Dynamics at the Porphyrin/Ag Interface. *J. Phys. Chem. Lett.* **2015**, *6*, 3632−3638.
50. Zei, M. S.; Nakai, Y.; Lehmpfuhl, G.; Kolb, D. M. The structure of gold and silver films evaporated on glass: A leed and rheed study. *J. Electroanal. Chem.* **1983**, *150*, 201−208.
51. Uosaki, K.; Ye, S.; Kondo, T. *J. Phys. Chem.* **1995**, *99*, 14117−14122.

52. Uosaki, K.; Ye, S.; Naohara, H.; Oda, Y.; Haba, T.; Kondo, T. Electrochemical epitaxial growth of a Pt(111) phase on an Au(111) electrode. *J. Phys. Chem. B* **1997**, *101*, 7566−7572.
53. Uosaki, K.; Ye, S.; Oda, Y.; Haba, T.; Hamada, K. Adsorption of Hexachloroplatinate Complex on Au(111) Electrode. An in situ Scanning Tunneling Microscopy and Electrochemical Quartz Microbalance Study. *Langmuir*, **1997**, *13*, 594−596.
54. Ye, S.; Ishibashi, C.; Shimazu, K.; Uosaki, K. An In Situ Electrochemical Quartz Crystal Microbalance Study of the Dissolution Process of a Gold Electrode in Perchloric Acid Solution Containing Chloride Ion. *J. Electrochem. Soc.* **1998**, *145*, 1614−1623.
55. Kresse, G.; Hafner, J. Ab Initio Molecular Dynamics for Liquid Metals. *Phys. Rev. B* **1993**, *47*, 558−561.
56. Kresse, G.; Hafner, J. Ab Initio Molecular-Dynamics Simulation of the Liquid-Metal Amorphous-Semiconductor Transition in Germanium. *Phys. Rev. B* **1994**, *49*, 14251−14269.
57. Kresse, G.; Furthmüller, J. Efficient Iterative Schemes for Ab Initio Total-Energy Calculations Using a Plane-Wave Basis Set. *Phys. Rev. B* **1996**, *54*, 11169−11186.
58. Kresse, G.; Furthmüller, J. Efficiency of Ab-Initio Total Energy Calculations for Metals and Semiconductors Using a Plane-Wave Basis Set. *Comput. Mater. Sci.* **1996**, *6*, 15−50.
59. Perdew, J. P.; Burke, K.; Ernzerhof, M. Generalized Gradient Approximation Made Simple. *Phys. Rev. Lett.* **1996**, *77*, 3865−3868.
60. Perdew, J.; Burke, K.; Ernzerhof, M. Generalized Gradient Approximation Made Simple [Erratum Phys. Rev. Lett. 77, 3865 (1996)]. *Phys. Rev. Lett.* **1997**, *78*, 1396−1396.
61. Grimme, S.; Antony, J.; Ehrlich, S.; Krieg, H. A consistent and accurate ab initio parametrization of density functional dispersion correction (DFT-D) for the 94 elements H-Pu. *J. Chem. Phys.* **2010**, *132*, No. 154104.

62. Blöchl, P. E. Projector augmented-wave method. *Phys. Rev. B* **1994**, *50*, 17953−17979.
63. Kresse, G.; Joubert, D. From Ultrafast Pseudopotentials to the Projector Augmented-Wave Method. *Phys. Rev. B: Condens. Matter Mater. Phys.* **1999**, *59*, 1758−1775.
64. Methfessel, M.; Paxton, A. T. High-precision sampling for Brillouin-zone integration in metals. *Phys. Rev. B* **1989**, *40*, 3616−3621.
65. Monkhorst, H. J.; Pack, J. D. Special Points for Brillouin-zone Integrations. *Phys. Rev. B* **1976**, *13*, 5188−5192.
66. *Handbook of Chemistry and Physics*; Lide, D. R., Ed.; CRC Press: Boca Raton, FL, 2008; pp 12−15.
67. Giannozzi, P.; Baroni, S. Vibrational and Dielectric Properties of C_{60} from Density-Functional Perturbation Theory. *J. Chem. Phys.* **1994**, *100*, 8537−8539.
68. Baroni, S.; de Gironcoli, S.; Dal Corso, A.; Giannozzi, P. Phonons and Related Crystal Properties From Density-Functional Perturbation Theory, *Rev. Mod. Phys.* **2001**, *73*, 515.
69. Lee, S.-S.; Kim, B.; Lee, S. Structures and Bonding Properties of Gold–Arg-Cys Complexes: DFT Study of Simple Peptide-Coated Metal. *J. Phys. Chem. C* **2014**, *118*, 20840−20847.
70. Seydou, M.; Teyssandier, J.; Battaglini, N.; Kenfack, G. T.; Lang, P.; Tielens, F.; Maurel F.; Diawara, B. Characterization of NTCDI Supra-Molecular Networks on Au(111); Combining STM, IR and DFT Calculations. *RSC Adv.* **2014**, *4*, 25698−25708.
71. Davantès, A.; Costa, D.; Lefèvre, G. Infrared Study of (Poly)Tungstate Ions in Solution and Sorbed into Layered Double Hydroxides: Vibrational Calculations and In Situ Analysis. *J. Phys. Chem. C* **2015**, *119*, 12356−12364.
72. Garrido Torres, J. A.; Götze, J. P.; Grillo, F.; Richardson, N. V.; Früchtl, H.; Hooley, C. A.; Schaub, R. Calculating the frequencies and intensities of strongly anharmonic modes of

adsorbates on surfaces: A low-cost but accurate computational approach. *Phys. Rev. B* **2019**, *100*, 035433.

73. Pritchard, B. P.; Altarawy, D.; Didier, B.; Gibson, T. D.; Windus, T. L. New Basis Set Exchange: An Open, Up-to-Date Resource for the Molecular Sciences Community. *J. Chem. Inf. Model.* **2019**, *59*, 4814−4820.
74. Jorge, F.; Sagrillo, P.; de Oliveira, A. Gaussian Basis Sets of 5 Zeta Valence Quality for Correlated Wave Functions. *Chem. Phys. Lett.* **2006**, *432*, 558−563.
75. Barbieri, P. L.; Fantin, P. A.; Jorge, F. E. Gaussian Basis Sets of Triple and Quadruple Zeta Valence Quality for Correlated Wave Functions. *Mol. Phys.* **2006**, *104*, 2945−2954.
76. Machado, S. F.; Camiletti, G. G.; Canal Neto, A.; Jorge, F. E.; Jorge, R. S. Gaussian basis set of triple zeta valence quality for the atoms from K to Kr: Application in DFT and CCSD(T) calculations of molecular properties. *Mol. Phys.* **2009**, *107*, 1713−1727.
77. Canal Neto, A.; Muniz, E.P.; Centoducatte, R.; Jorge, F.E. Gaussian Basis Sets for Correlated Wave Functions. Hydrogen, Helium, First- and Second-row Atoms. *J. Mol. Struct.: THEOCHEM* **2005**, *718*, 219−224.
78. Dronskowski, R.; Blöchl, P. E. Crystal Orbital Hamilton Populations (COHP): Energy-Resolved Visualization of Chemical Bonding in Solids Based on Density-Functional Calculations. *J. Phys. Chem.* **1993**, *97*, 8617−8624.
79. Deringer, V. L.; Tchougréeff, A. L.; Dronskowski, R. Crystal Orbital Hamilton Population (COHP) Analysis as Projected from Plane-Wave Basis Sets. *J. Phys. Chem. A* **2011**, *115*, 5461−5466.

80. Maintz, S.; Deringer, V. L.; Tchougréeff, A. L.; Dronskowski, R. Analytic Projection from Plane-Wave and PAW Wavefunctions and Application to Chemical-Bonding Analysis in Solids. *J. Comput. Chem.* **2013**, *34*, 2557−2567.
81. Maintz, S.; Deringer, V. L.; Tchougréeff, A. L.; Dronskowski, R. LOBSTER: A Tool to Extract Chemical Bonding from Plane-Wave Based DFT. *J. Comput. Chem.* **2016**, *37*, 1030−1035.
82. Steinberg, S.; Dronskowski, R. The Crystal Orbital Hamilton Population (COHP) Method as a Tool to Visualize and Analyze Chemical Bonding in Intermetallic Compounds. *Crystals* **2018**, *8*, 225.
83. Momma, K.; Izumi, F. VESTA 3 for Three-dimensional Visualization of Crystal, Volumetric and Morphology data. *J. Appl. Crystallogr.* **2011**, *44*, 1272.
84. Li, Y.; Lu, D.; Swanson, S. A.; Scott, J. C.; Galli, G. Microscopic Characterization of the Interface between Aromatic Isocyanides and Au(111): A First-Principles Investigation. *J. Phys. Chem. C* **2008**, *112*, 6413−6421.
85. Gilman, Y.; Allen, P. B.; Hybertsen, M. S. Density-Functional Study of Adsorption of Isocyanides on a Gold (111) Surface. *J. Phys. Chem. C* **2008**, *112*, 3314−3320.
86. Astruc, D. Organometallic Chemistry and Catalysis, Springer, Berlin, 2007, p. 608.

Supporting Information

Identifying Substrate-Dependent Chemical Bonding Nature at Molecule/Metal Interfaces Using Vibrational Sum Frequency Generation Spectroscopy and Theoretical Calculations

Ben Wang,[†] Mikio Ito,[#] Min Gao,[§] Hidenori Noguchi,[$]

Kohei Uosaki,[$,*] and Tetsuya Taketsugu[†,ǁ,*]

[†]*Department of Chemistry, Faculty of Science, Hokkaido University, Sapporo 060-0810, Japan*

[#]*Department of Chemical Science and Engineering, National Institute of Technology, Tokyo College, 1220-2 Kunugida-machi, Hachioji, Tokyo 193-0997, Japan*

[§]*Institute for Catalysis, Hokkaido University, Sapporo 001-0021, Japan*

[$]*Center for Global Research on Energy and Environmental Materials (GREEN), National Institute for Materials Science (NIMS), Tsukuba 305-0044, Japan*

[ǁ]*Institute for Chemical Reaction Design and Discovery (WPI-ICReDD), Hokkaido University, Sapporo 001-0021, Japan*

Table S1. Parameters for fitting the VSFG spectra shown in Figure 1 using eqn (2). The Hammett constants for the substituents are also given.

		NO_2	H	OCH_3
	σ_p	0.78	0	−0.27
Au	A	2.2	2.4	4.7
	ν_{NC}	2194	2199	2194
	Γ	10	14	11
	$\chi_{NR}^{(2)}$	0.40	0.49	0.56
	ϕ	−146	−120	−130
Ag	A	0.49	3.8	1.4
	ν_{NC}	2176	2186	2185
	Γ	11	14	7.1
	$\chi_{NR}^{(2)}$	0.63	1.8	1.5
	ϕ	−121	−118	−139

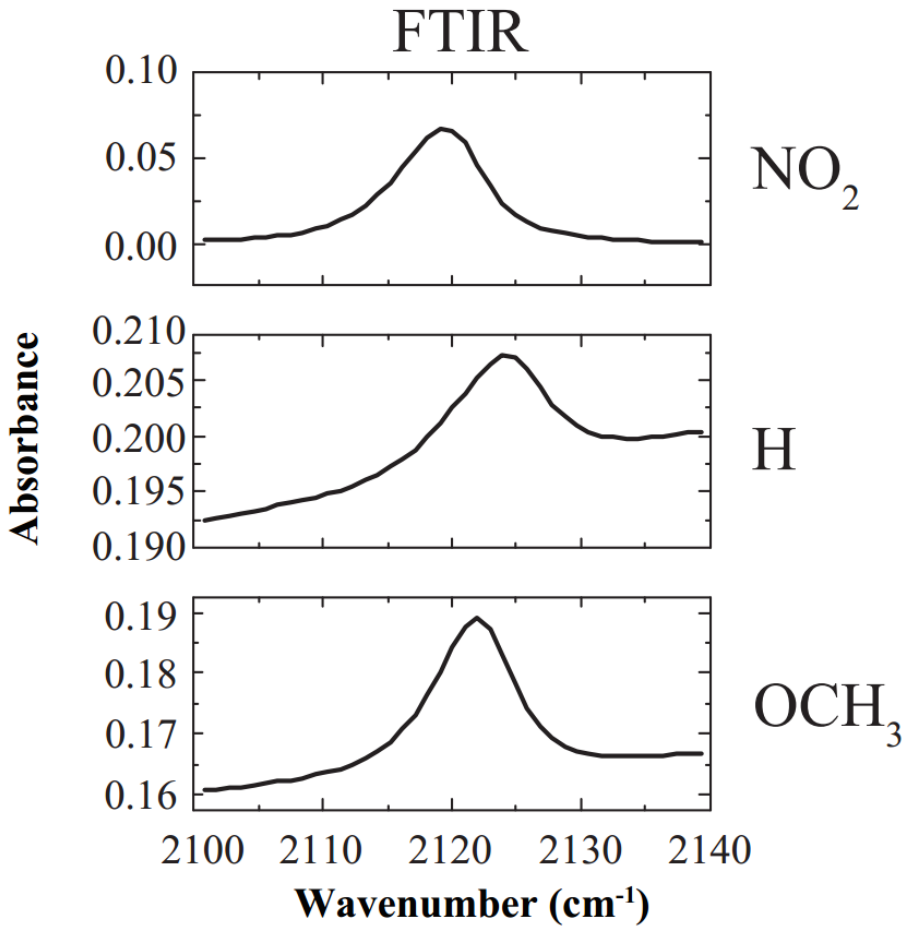

Figure S1. Results of FTIR spectroscopy measurement for isolated $NO_2{-}C_6H_4{-}NC$, $H{-}C_6H_4{-}NC$, and $OCH_3{-}C_6H_4{-}NC$ molecules, respectively.

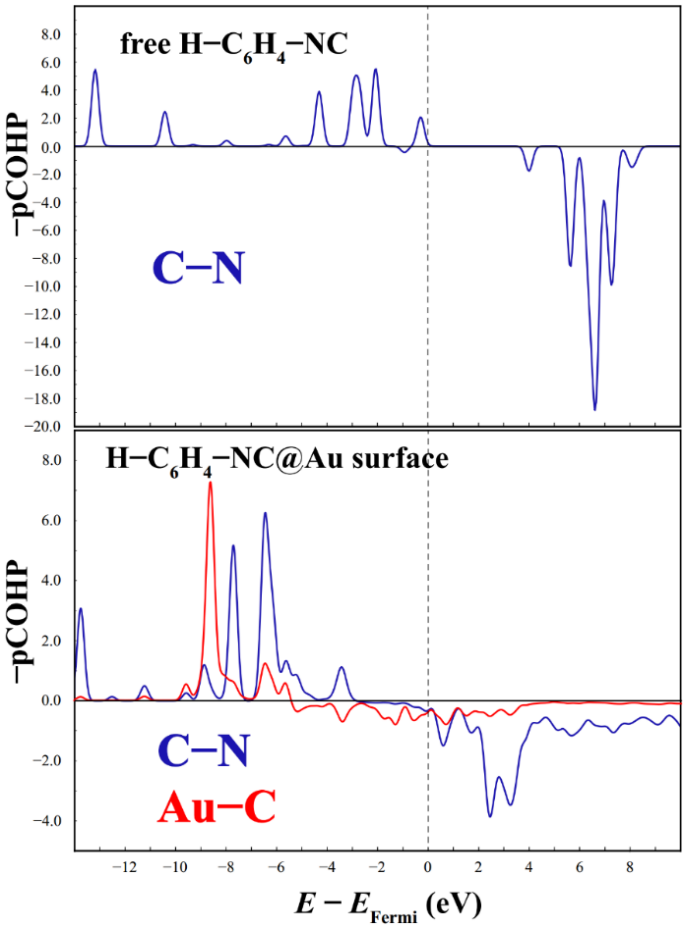

Figure S2. −pCOHP plots for free H−C_6H_4−NC molecule and H−C_6H_4−NC molecule adsorbed on Au surface, C−N and Au−C interactions have been highlighted by blue and red colors, respectively.

After binding to the Au surface, the 5σ-d state, the 1π-d state, and the 2π*-d state with bonding and antibonding characters were identified by COHP analysis. The difference in the orbitals obtained by NBO and COHP (also PDOS) was induced by different algorithms. According to reference [J. Chem. Theory Comput. 2012, 8, 6, 1902], COHP is a method based on reciprocal space and is used to describe delocalized interactions analysis. NBO converts atomic orbital to hybrid orbitals, perhaps not very close to atomic orbitals, provides a purely localized real space representation of bonding interactions and allows one to find the intrinsic localization in the system. Therefore, the COHP analysis possibly gave an orbital-interaction picture compared to the NBO analysis.

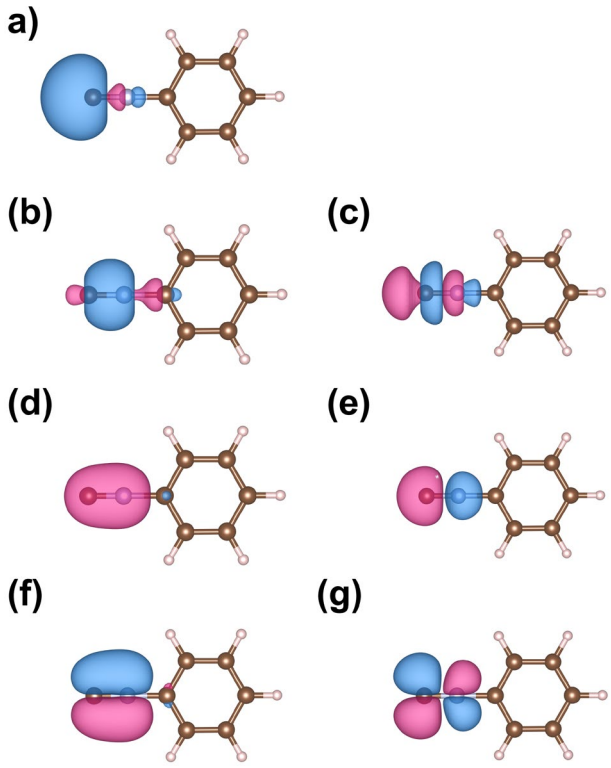

Figure S3. NBOs of isolated H−C_6H_4−NC molecule: a) The lone pair 5σ orbital localized at C atom, b, c) NC σ bonding and σ* antibonding orbitals, d, e) out-of-plane NC 1π bonding and 2π* antibonding orbitals, f, g) in-plane NC 1π bonding and 2π* antibonding orbitals. An isosurface value of 0.035 *e*/Bohr^3 is used.

Table S2. NBO occupancies of NC σ bonding and NC σ* antibonding orbitals calculated for isolated H−C_6H_4−NC molecule and H−C_6H_4−NC molecule adsorbed on Au(111) or Ag(111) surfaces.

	NC σ	NC σ*
free	1.9875	0.0058
on Au	1.9797	0.0139
on Ag	1.9800	0.0110

Table S3. NBO occupancy analysis conducted for NO_2−C_6H_4−NC and OCH_3−C_6H_4−NC as free molecules and those adsorbed on Au and Ag surfaces.

		metal-C σ	metal-C σ*	NC π	NC π*	NC σ	NC σ*
free	NO_2	/	/	3.8979	0.0740	1.9875	0.0056
	OCH_3	/	/	3.9188	0.0941	1.9872	0.0057
on Au	NO_2	1.8354	0.1021	3.8914	0.3809	1.9799	0.0138
	OCH_3	1.8365	0.1033	3.8974	0.3746	1.9798	0.0137
on Ag	NO_2	1.8504	0.0743	3.8939	0.3322	1.9804	0.0107
	OCH_3	1.8518	0.0741	3.8883	0.3398	1.9795	0.0111

Similar with our previous work aimed at the benchmark of substituent effect (*Phys. Chem. Chem. Phys*. **2020**, *22*, 12200−12208), the substituted group effect on NBO orbitals was analyzed and summarized in Table S3. In our previous results, compared to the substitute group ─H, electron withdrawing groups increase the occupation of ─NC π* and σ*, therefore decrease the bond order of ─NC. While the electron donating group does affect ─NC bond strongly.

Table S4. NBO occupancies (*e*) in several typical orbitals when projecting on various different basis set combinations for adsorbed molecules.

Basis Set Test					
		a	**b**	**c**	**d**
H−C_6H_4−NC @Au surface	Au−C σ	1.8407	1.8384	1.8369	1.8347
	Au−C σ*	0.1059	0.1065	0.1031	0.1061
	C−N σ	1.9797	1.9643	1.9550	1.9631
	C−N σ*	0.0139	0.0131	0.0147	0.0138
	C−N π	3.8931	3.8842	3.8818	3.8840
	C−N π*	0.3650	0.3609	0.3755	0.3729

a. Au: jorge-DZP; C, H, N: jorge-DZP (original manuscript)
b. Au: jorge-DZP; C, H, N: jorge-TZP
c. Au: jorge-DZP; C, H, N: def2-TZVPP
d. Au: jorge-DZP; C, H, N: Sapporo-TZP

To investigate the influence of basis sets, the current periodic NBO program can only project plane-wave basis sets to Gaussian basis sets including S, P, D, F, and SP orbital types, and the projection to G-type orbitals for Au and Ag atoms (triple-ζ basis set) is currently not supported by the periodic NBO algorithm. Therefore, different basis sets were considered for adsorbed molecules shown in Table S4. The results indicate that the performance of TZP is comparable in quality to the DZP results. Increasing the TZP basis set does not necessarily improve the quality of the results, and a double-ζ basis set seems to be sufficient for this projection.

Table S5. Comparison of various charge models (Bader, NPA, Hirshfeld, and DDEC6) for H−C_6H_4−NC on Au surface (unit: *e*). Values in parentheses are the corresponding charges ***before*** adsorption.

	adsorbing Au atom	all metal atoms	C	N	molecule
Bader	0.15 (−0.02)	−0.02 (0)	0.83 (0.83)	−1.42 (−1.52)	0.02 (0)
NPA	−0.35 (0.07)	−0.23 (0)	0.39 (0.26)	−0.37 (−0.49)	0.23 (0)
Hirshfeld	0.08 (0.01)	−0.06 (0)	−0.01 (−0.10)	−0.04 (−0.06)	0.06 (0)
DDEC6	0.07 (0.01)	−0.16 (0)	0.06 (−0.17)	−0.07 (−0.05)	0.16 (0)

Bader: VASP + Bader program developed by Henkelman group

NPA: VASP featured with periodic NBO

Hirshfeld: VASP package

DDEC6: VASP's charge density analyzed by Chargemol program

Table S5 compares Bader's charge results with those of the charge analysis by Natural Population Analysis (NPA), Hirshfeld, and DDEC6 using the same electron densities and wave functions. The results show that the directly bonded Au atoms lose electrons and become positively charged, while the entire metal surface accepts electrons and becomes negatively charged by −0.02 *e* according to the Bader charge. This indicates that the closer to other Au atoms, the higher the electron density. All four charge models indicate that the entire surface is negatively charged, and the adsorbate positively charged, with a slightly stronger tendency for electron transfer from the adsorbate to the surface. This is consistent with benchmark work on the partial atomic charges of metal atoms in transition metal complexes calculated with the Bader, Hirshfeld, CM5, DDEC3, and DDEC6 charge models (*J. Chem. Theory Comput.* **2020**, *16*, 5884). The maximum charge is also given in this benchmark work.

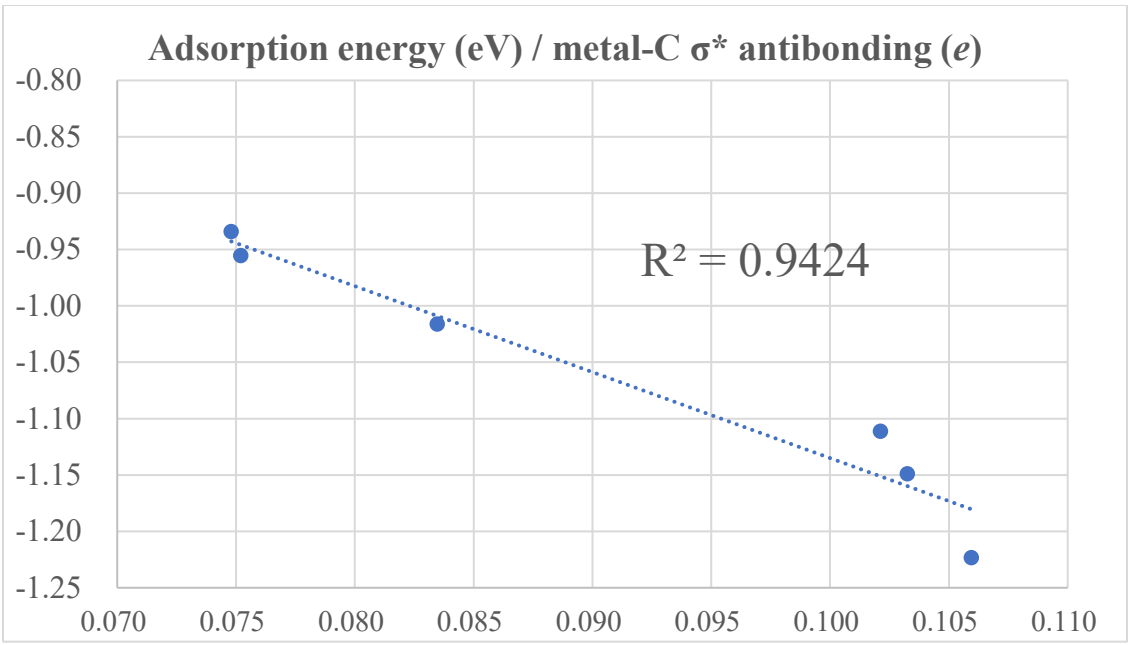

Figure S4. Adsorption energy as a function of NBO occupancy in metal-C σ* antibonding (named 5σ-d antibonding orbital in PDOS and -COHP analysis) for adsorption on atop site of Au and Ag surfaces.